Available online at www.sciencedirect.com
ScienceDirect
Ceramics International 36 (2010) 291–297
CERAMICS INTERNATIONAL
www.elsevier.com/locate/ceramint

Synthesis, characterization and bioactivity investigation of bioglass/hydroxyapatite composite

R. Ravarian [a,*], F. Moztarzadeh [a], M. Solati Hashjin [a], S.M. Rabiee [b], P. Khoshakhlagh [a], M. Tahriri [a]

[a] *Amirkabir University of Technology, Faculty of Biomedical Engineering, Biomaterial Group, P.O. Box 15875-4413, Tehran, Iran*
[b] *Mechanical Engineering Department, Babol Noshirvani University of Technology, Babol, Iran*

Received 23 March 2009; received in revised form 13 May 2009; accepted 29 July 2009
Available online 23 September 2009

Abstract

Bioactive glass of the type $CaO–P_2O_5–SiO_2$ was obtained by the sol–gel processing method. The obtained material was characterized by X-ray powder diffraction (XRD). Composite samples of hydroxyapatite with synthesized bioglass were prepared at 1000 °C and characterized by XRD, Fourier transform infrared spectroscopy (FTIR), and surface electron microscopy (SEM). The bioactivity was examined *in vitro* with respect to the ability of hydroxyapatite layer to form on the surface as a result of contact with simulated body fluid (SBF). XRD, FTIR and SEM studies were conducted before and after contact of the material with SBF. It could be detected that the bioglass was crystallized partly. Furthermore, silicated hydroxyapatite may have formed due to the diffusion of silicate groups to the apatite phase and these may have substituted for the phosphate groups. It can be concluded from SEM and FTIR results that apatite phase formed after 14 days in SBF.

Keywords: A. Sol–gel processes; B. Composites; D. Bioglass; D. Hydroxyapatite

1. Introduction

Bioactive glasses were discovered in 1969 and provided for the first time an alternative; second generation, interfacial bonding of an implant with host tissues [1]. Autologous bone grafts are considered the gold standard in bone repair and regeneration because of their osteogenicity, osteoinductivity and osteoconduction [2]. Glasses and glass-ceramics based on the $SiO_2–CaO–P_2O_5$ system constitute an important group of materials that have found wide application in medicine as bone implants [4].

When in contact with body fluids or tissues, bioactive glasses develop reactive layers at their surfaces resulting in a chemical bond between implant and host tissue [5]. Hench and co-workers have described a sequence of five reactions that result in the formation of a hydroxy-carbonate (HCA) apatite layer on the surface of these bioactive glasses [3,6,7]. The dissolution of the glass network, leading to the formation of a silica-rich gel layer and subsequent deposition of an apatite-like layer on the glass surface, was found to be essential steps for bonding of glass to living tissues both through *in vivo* and *in vitro* studies [8].

Sol–gel processing has been successfully used in the production of a variety of materials for both biomedical and nonbiomedical applications [9]. Sol–gel processing, an alternative to traditional melt processing of glasses, involves the synthesis of a solution (sol), typically composed of metal-organic and metal salt precursors followed by the formation of a gel by chemical reaction or aggregation, and lastly thermal treatment for drying, organic removal, and sometimes crystallization [10]. Sol–gel-derived bioactive glasses were used because they exhibit high specific area, high osteoconductive properties, and a significant degradability [11]. The sol–gel approach to making bioactive glass materials has produced glasses with enhanced compositional range of bioactivity [8]. Bioactive glass-ceramics composed of very small grain sizes of apatite and wollastonite crystal phases in a silicate glassy grain boundary phase are mechanically strong and tough as well as being bone bonding [12].

Hydroxyapatite (HA) belongs to a group of calcium phosphates, which are being considered as bone substitute

* Corresponding author. Tel.: +98 261 2814911.
E-mail address: ravarian@gmail.com (R. Ravarian).

0272-8842/$36.00
doi:10.1016/j.ceramint.2009.09.016

materials, which will not cause defensive bodily reactions, and will even establish interactions with the body. The composition of HA is $Ca_5(PO_4)_3OH$ with a Ca/P molar ratio equivalent to 1.67 [13].

Even if the biocompatibility of HA is excellent, its bioactivity can be improved. One way to increase it would be to use the ability of the apatite to accept many substituting ions in its unit cell [14]. These ionic substitutions can affect the surface-structure and charge of hydroxyapatite, which would have an influence on the material in biological environments. In this sense, an interesting way to improve the bioactivity of hydroxyapatite is the addition of silicon to the apatite structure, taking into account the influence of this element on the bioactivity of bioactive glasses and glass-ceramics [15–20]. Several authors reported the improved bioactivity and dissolution rate of HA in the presence of silicon [21–29].

It has been observed that the addition of Si during the HA synthesis leads to an improvement of the bioactive behavior. The silanol groups in glass-ceramics or bioglass have been proposed as catalysts of the apatite phase nucleation in forming surface apatite layers [30–33]. A method for substituting silicate ions into the HA lattice has been developed with the hypothesis that sitespecific substitution of silicate ions (SiO_4^{4-}) for phosphate ions (PO_4^{3-}) at ultra-trace levels will enhance the bioactivity of HA through either its effect on surface chemistry (surface availability of Si and its influence on surface charge) or controlled local bioavailable Si release [17].

The advantage of using HA as a bioceramic or biomaterial compared to other bioceramics, such as bioglass or A-W glass-ceramic, is its chemical similarity to the inorganic component of bone and tooth. However, the disadvantage of using HA as an implant in comparison with bioactive glasses and ceramics is that its reactivity with existing bone is low, and the rate at which bone apposes and integrates with HA is relatively low [15].

Kokubo et al. [34] developed a series of acellular aqueous solutions, which are able to reproduce *in vivo* surface-structure changes in bioactive materials. The SBF solution is the close to the ion composition of human plasma, as shown in Table 1 [35].

The apatite layer is formed on the surface when these materials are soaked in solutions mimicking plasma. *In vitro* studies have shown that the apatite formation on gel glasses depends on several factors including the glass composition, its textural properties (specific surface area, porosity), and the composition of the assay solution [36].

Table 1
Composition of SBF and the inorganic part of human blood plasma (mmol/l).

Ion	Plasma (mmol/l)	SBF (mmol/l)
Na^+	142.0	142.0
K^+	5.0	5.0
Mg^{2+}	1.5	1.5
Ca^{2+}	2.5	2.5
Cl^-	103.0	147.8
HCO_3^-	27	4.2
HPO_4^{2-}	1.0	1.0
SO_4^{2-}	0.5	0.5

Therefore, in this study, the effect of HA addition into a $CaO–SiO_2–P_2O_5$ bioglass on bioactivity has been investigated.

2. Materials and methods

Glass materials $SiO_2–P_2O_5–CaO$ (64% SiO_2, 31% CaO, and 5% P_2O_5), (based on mol.%), were synthesized by the sol–gel method and characterized by X-ray diffraction (XRD) analysis. Furthermore, HA/bioglass composite samples were prepared and again characterized by XRD and Fourier transform infrared spectroscopy (FTIR) and scanning electron microscopy (SEM). In addition, the *in vitro* bioactivity was evaluated by soaking of samples in simulated body fluid (SBF). Finally, the samples were again analyzed to quantify the apatite forming ability upon soaking in SBF solution.

2.1. Synthesis of bioglass

In the first step, the solution was prepared as follows: 13.33 g (0.064 mol) of tetraethyl orthosilicate (TEOS; Merck) was added into 30 ml of 0.1 M nitric acid (Merck); the mixing process was allowed to be continued for 30 min for the acid hydrolysis of TEOS to proceed almost to completion. The following reagents were added in sequence. About 45 min were given to each reagent to react thoroughly: 0.91 g (0.005 mol) triethyl phosphate (TEP; Merck), 7.32 g (0.031 mol) of calcium nitrate tetrahydrate (Merck). To allow completion of the hydrolysis reaction, mixing was continued for 1 h after the last addition. The solution was cast in a cylindrical teflon container and kept sealed for 10 days at room temperature to allow the hydrolysis and polycondensation reactions to take place until the gel was formed. The gel was kept in a sealed container and heated at 70 °C for 3 days. To get rid of the water a small hole was contrived in the lid to allow the leakage of gases while heating the gel to 120 °C for 3 days to remove all the water. The dried gel was then heated for 24 h at 700 °C for two reasons first to stabilize the glass and second to eliminate residual nitrate [10].

2.2. Specimen preparation

Prepared bioglass was mixed with different ratios of HA as listed in Table 2. HA powder was used as-received from Plasma Biotal Ltd. and its trade name was Captal.

Powder of bioglass/HA, with various weight ratios, was prepared in a planetary ball mil (Retch PMA, Brinkman, USA) for 30 min to ensure homogeneity. The powder (P) was suspended in distilled water (W) at a ratio of P/W = 45% (w/v). the mixture were stirred for 12 h to make a suitable ceramic

Table 2
Prepared samples of bioglass/HA composite.

Sample code	Bioglass (wt%)	HA (wt%)
B10	100	0
B9	90	10
B8	80	20
B7	70	30

slurry. Samples were prepared by foaming method. Polymeric foam was cut into 1 cm × 1 cm × 1 cm and was soaked in the slurry. Samples were dried in an ambient temperature for 48 h.

Samples were heated up to 1000 °C for sintering with the following parameters: heated to 200 °C at 2 °C/min, to 600 °C at 0.5 °C/min, remained in 600 °C for 1 h, to 1000 °C at 5 °C/min. Samples were kept for 3 h in 1000 °C then they were cooled down in the furnace to avoid thermal shocks. Rate of thermal decrease was 5 °C/min.

2.3. Preparation of SBF

The SBF solution was prepared by dissolving reagent-grade NaCl, KCl, $NaHCO_3$, $MgCl_2{\cdot}6H_2O$, $CaCl_2$ and KH_2PO_4 into distilled water and buffered at pH 7.25 with trishydroxymethyl aminomethane (TRIS) and HCl 1N at 37 °C. Its composition is given in Table 1 and is compared with the ionic composition of human blood plasma [10].

2.4. Sample characterization

2.4.1. X-ray diffraction (XRD)

For X-ray diffraction analysis, the sintered samples were grinded and powdered. The resulting powders were analyzed with a Philips PW 3710. X-ray diffractometer, with voltage and current settings of 30 kV and 25 mA, respectively and with Cu Kα radiation (1.5405 Å). For qualitative analysis, XRD patterns were recorded in the interval $20^\circ \leq 2\theta \leq 50^\circ$ at a scan speed of 2°/min. Step size which was used was 0.02°.

2.4.2. Fourier transform infrared spectroscopy (FTIR)

The grinded samples were examined by Fourier transform infrared spectroscopy by the use of a Thermo Nicolet (USA) FTIR spectrometer. For IR analysis, 1 mg of the powder samples were carefully mixed with 300 mg of KBr (infrared grade) and pelletized under vacuum. Then the pellets were analyzed in the range of 400–4000 cm^{-1} at the scan speed of 23 scan/min with 4 cm^{-1} resolution.

2.4.3. Scanning electron microscopy (SEM)

The samples were coated with a thin layer of gold (Au) by sputtering (EMITECH K450X, England) and then the microstructures were observed using a scanning electron microscope (VEGA TESCAN 2XMU) that operated at the acceleration voltage of 15 kV.

Table 3
Sample codes including incubation time in SBF.

Incubation time in SBF	B10	B9	B8	B7
0 (not being soaked in SBF)	B10-0D	B9-0D	B8-0D	B7-0D
14 days	B10-14D	B9-14D	B8-14D	B7-14D

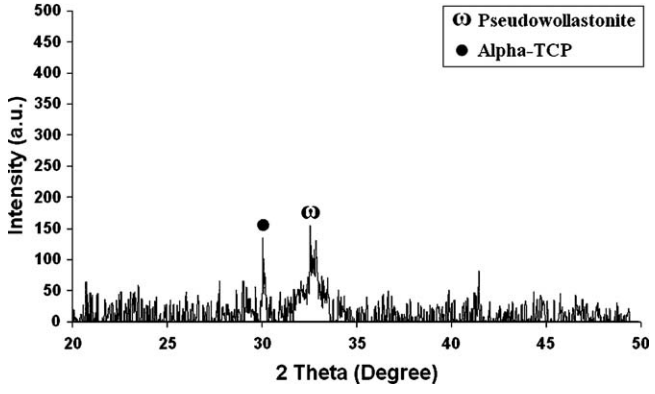

Fig. 1. Bioglass XRD pattern after thermal treatment at 700 °C.

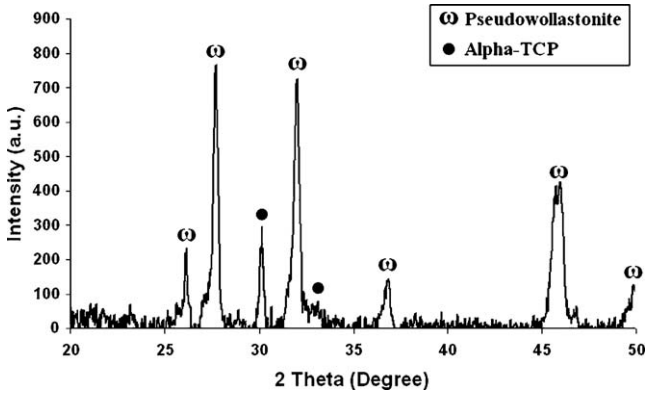

Fig. 2. XRD pattern of sample B10-0D.

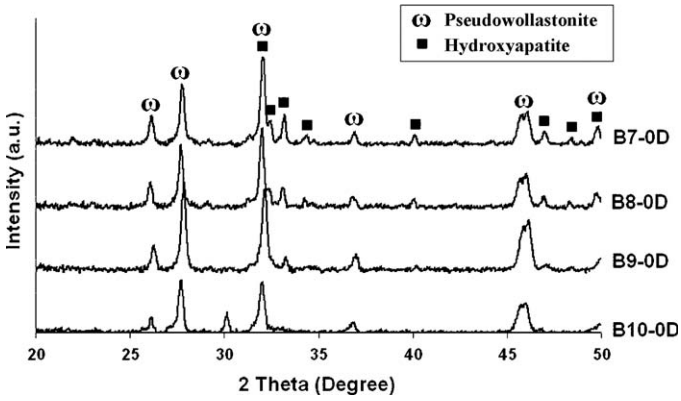

Fig. 3. The XRD pattern of composite samples before soaking in SBF.

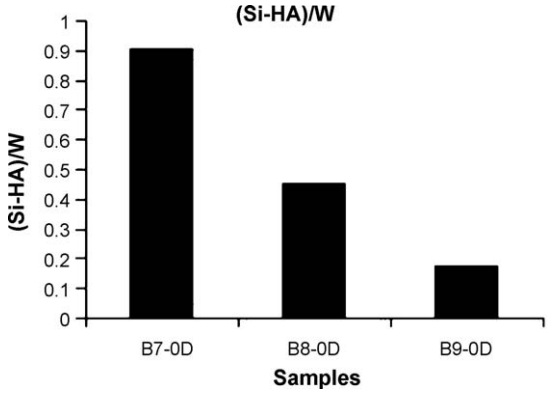

Fig. 4. The ratio of silicate hydroxyapatite to pseudowollastonite in samples B9, B8 and B7.

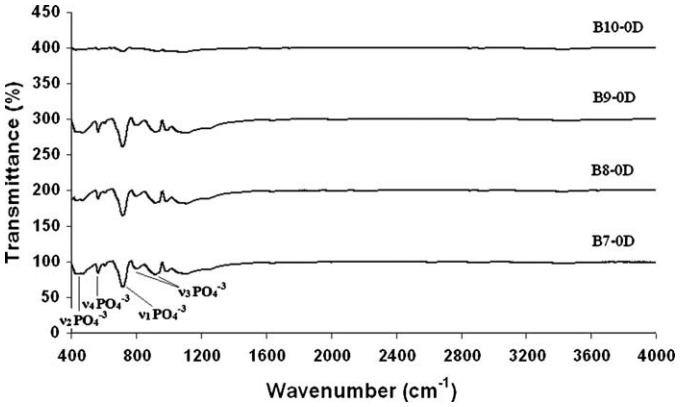

Fig. 5. FTIR results of the samples before soaking in SBF.

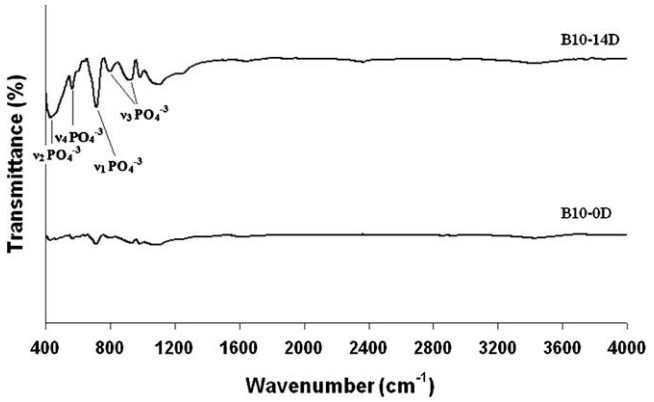

Fig. 6. FTIR results of sample B10 before and after soaking in SBF for 14 days.

2.4.4. *In vitro studies in SBF*

In vitro studies were carried out by soaking the samples (listed in Table 2) in SBF at 37 °C for intervals of 0 (without soaking in SBF) and 14 days. Therefore, new codes have been given to the samples including their incubation time in SBF. Table 3 shows the given codes. B10-0D, B9-0D, B8-0D and B7-0D are the codes, which were given to the samples in Table 2. The results will be discussed using codes in Table 3. After

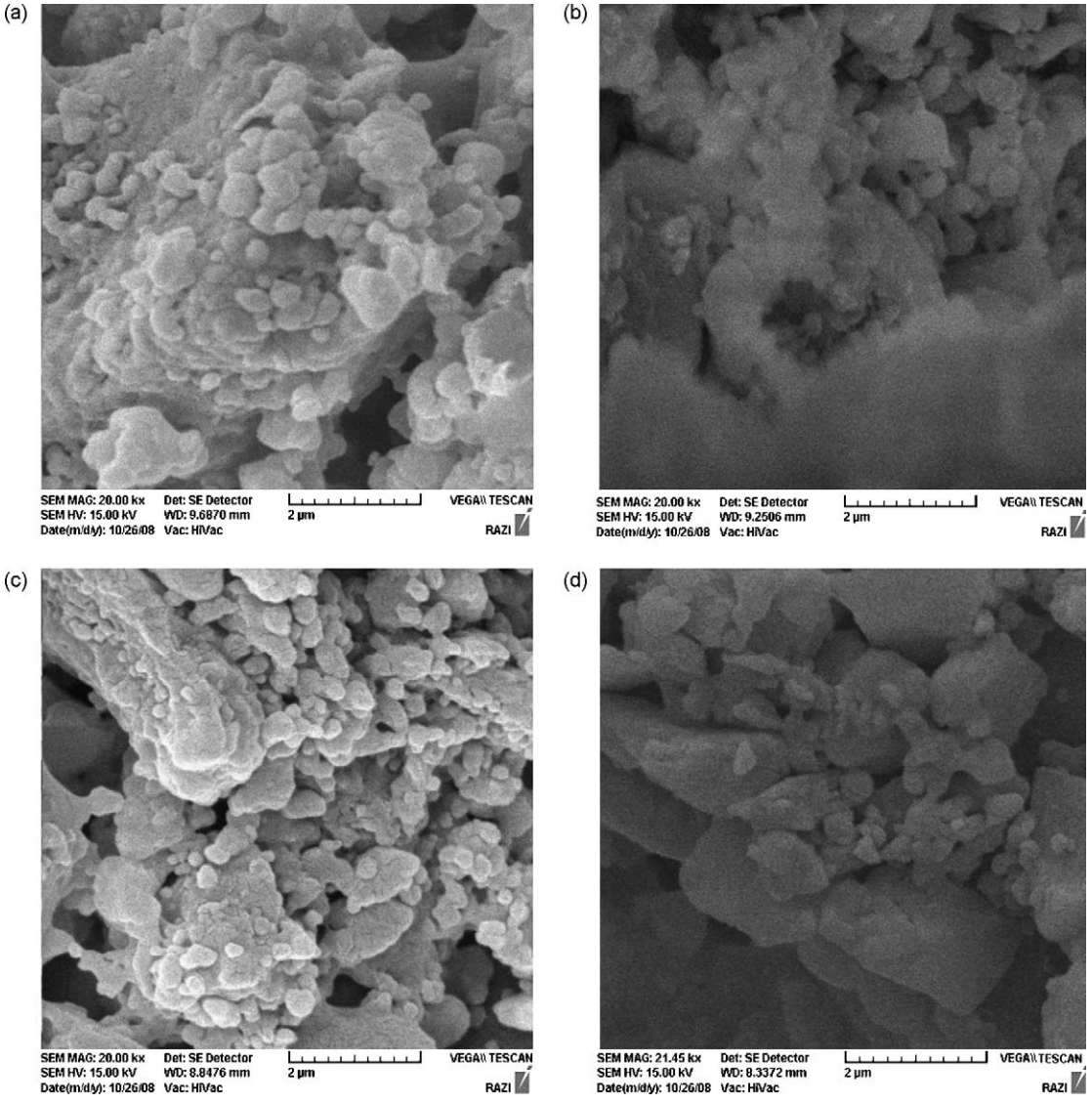

Fig. 7. SEM images of samples before soaking in SBF (a) B7-0D (b) B8-0D (c) B9-0D (d) B10-0D.

soaking, the powder was filtered, rinsed with doubly distilled water, and dried in an oven at 120 °C for 12 h before analysis by FTIR and XRD and SEM.

3. Results and discussions

3.1. Phase characterization

The primary bioglass phases were investigated by X-ray diffraction. Fig. 1 shows the XRD pattern of bioglass, which has been produced after thermal treatment on 700 °C. As you can see in this figure, the bioglass is approximately amorphous. Regarding to the XRD patterns of the bioglass which is heated at 1000 °C (Fig. 2), it can be detected that at 700 °C, α-TCP and wollastonite (pseudowollastonite, JCPDS No.: 19-0248) have started to crystallize. It can be concluded that the synthesized bioglass has not been crystallized completely up to 700 °C.

The prepared samples of bioglass/HA composite were also investigated by X-ray diffraction. Samples B10, B9, B8 and B7 (all of the samples in Table 3) were characterized by XRD. The result of XRD analysis for sample B10-0D, which does not contain hydroxyapatite, can be seen in Fig. 2. XRD pattern of sample B10-0D, which contains 100% bioglass, shows that wollastonite has been formed. The presence of α-TCP phase is reasonable due to the existence of phosphate and silicate groups in bioglass structure and the high temperature (1000 °C) which is used in the process.

The XRD results of samples before being soaked in SBF (B10-0D, B9-0D, B8-0D and B7-0D) can be seen in Fig. 3. It can be concluded from this figure that the main phases of these samples are pseudowollastonite and hydroxyapatite (JCPDS No.: 090432). It can be concluded that the synthesized bioglass has been partly crystallized at 1000 °C. It has been reported that pseudowollastonite is a bioactive material, and its *in vitro* and *in vivo* tests have been investigated [36–40]. Pseudowollastonite

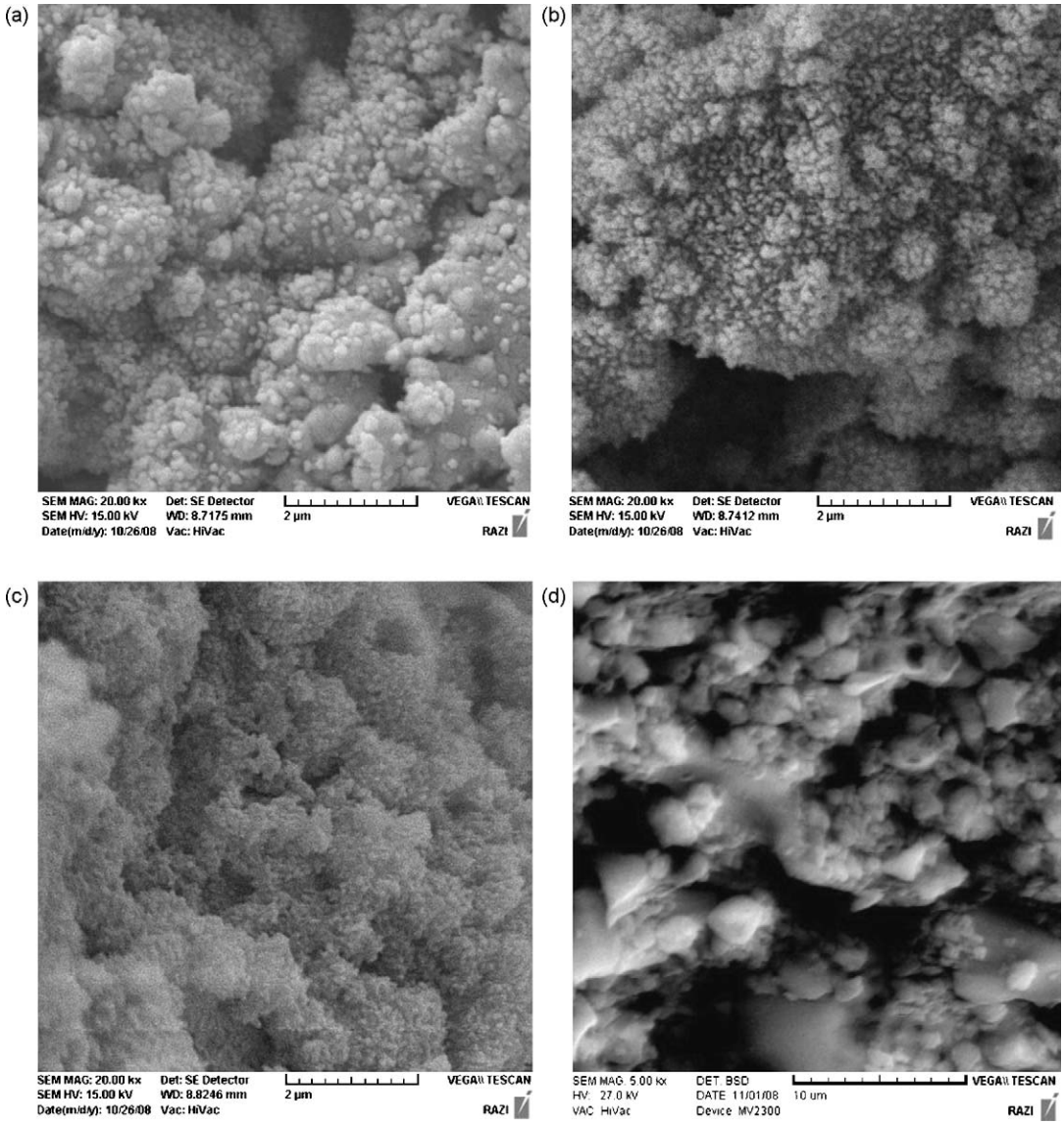

Fig. 8. SEM images of samples after soaking in SBF for 14 days. (a) B7-14D (b) B8-14D (c) B9-14D (d) B10-14D.

is a bioactive ceramic material that induces direct bone growth [41,42].

To compare the intensity of the formed phases, two characteristic peaks of pseudowollastonite and hydroxyapatite were selected for comparison. $2\theta = 36.80$ for wollastonite and $2\theta = 40.17$ for hydroxyapatite phase were selected and their intensities were compared. The results can be seen in Fig. 4. Obviously sample B7 has the most content of hydroxyapatite (silicated hydroxyapatite in fact as described later) and sample B9 has the least content of hydroxyapatite or it can be said that it has the most content of wollastonite.

Furthermore, the samples were investigated by FTIR. B10, B9, B8 and B7 were analyzed by FTIR. Fig. 5 demonstrates FTIR results of the samples before soaking in SBF.

There is a significant point in FTIR diagrams. Since there was a part of hydroxyapatite in the composition of prepared composite, it was expected to find the hydroxyl group peaks on 3570 cm^{-1}. However, as it can be seen in Fig. 5 the hydroxyl groups cannot be detected. It can be concluded that the HA is decomposed by the presence of glass, which enters the HA structure and causes the hydroxyl groups to be driven off [43]. The XRD peaks demonstrated HA peaks. This loss of OH groups may be due to silicon being incorporated in to the HA structure with silicate-substituted hydroxyapatite being formed, but may also be due to oxyapatite being formed. To verify this, further analysis of e.g. changes in unit cell parameters would be required. The negative charge of the silicate anions substituting phosphate ones was balanced by the creation of hydroxide vacancies, leading to the following chemical formula of SiHA:

$$Ca_{10}(PO_4)_{6-x}(SiO_4)_x(OH)_{2-x} \qquad \text{with} 0 \leq x \leq 2 \tag{1}$$

The procedure can be seen in Eq. (2). As silicon group enters the HA structure, there will be a charge imbalance, so the hydroxyl group leave the structure to remake the charge balance. Because of this phenomenon, the hydroxyl group peak cannot be seen in 3570 cm^{-1} in FTIR results [44].

$$\begin{pmatrix} P^{+5} \\ P^{+5} \end{pmatrix}^{x} + \begin{pmatrix} OH^{-} \\ OH^{-} \end{pmatrix} \overset{x_{Si^{+4}}}{\rightleftarrows} \begin{pmatrix} Si^{+4} \\ P^{+5} \end{pmatrix}^{/} + (V_{OH^{-}})^{\bullet} \tag{2}$$

It is proposed that the larger addition of glass gives a larger number of ions present, and these ions enter the HA structure and become interstitial ions.

3.2. In vitro assessment

Samples soaked in SBF were analyzed with XRD, FTIR and SEM. Soaking in SBF led to formation of an apatite layer on the surface of the samples, which can be seen both in FTIR and in SEM results. Fig. 6 shows the FTIR results, which compare B10 before and after soaking in SBF (B10-0D and B10-14D). Sample B10 was selected because it was completely free of HA, so the formation of HA because of soaking in SBF could be indicated clearly. It is quite obvious that phosphate groups (600–700 cm^{-1}) have been formed because of soaking in SBF for 14 days in 37 °C.

Morphological and textural properties of the biomaterials also indicate that soaking in SBF led to the formation of an apatite layer [31–33] on the surface of the samples. Figs. 7 and 8 are the images observed by SEM, which show the difference of the surface of the samples before and after soaking in SBF that can be used for comparison. In all of the samples there can be seen the apatite (as shown in FTIR results) particles which formed on the surface after soaking in SBF. It can be concluded from the images that larger amount of bioglass in the content of the samples led to form atom of smaller apatite particles on the surface. However, it needs more investigation to be proved.

4. Conclusion

As can be seen, the glass has a major effect on the structure of the HA. This is related to decomposition caused by the addition of the glass, which is highly reactive at high temperature and forces major chemical changes associated with the hydroxyl site. By using HA with bioglass, a silicated hydroxyapatite may have been produced, which is a highly bioactive material. Furthermore, bioactivity of the samples could be demonstrated from FTIR and SEM pictures.

References

[1] L.L. Hench, The story of bioglass, J. Mater. Sci. Mater. Med. 17 (2006) 967–978.
[2] B.H. Fellah, O. Gauthier, P. Weiss, D. Chappard, P. Layrolle, Osteogenicity of biphasic calcium phosphate ceramics and bone autograft in a goat model, Biomaterials 29 (2008) 1177–1188.
[3] J. Zhong, D.C. Greenspan, Processing and properties of sol–gel bioactive glasses, J. Biomed. Mater. Res. Appl. Biomater. 53 (2000) 694–701.
[4] A. Balamurugan, G. Balossier, J. Michel, S. Kannan, H. Benhayoune, A.H.S. Rebelo, J.M.F. Ferreira, Sol gel derived SiO_2–CaO–MgO–P_2O_5 bioglass system preparation and *in vitro* characterization, J. Biomed. Mater. Res. B: Appl. Biomater. 83B (2007) 546–553.
[5] H. Ylanen, K.H. Karlsson, A. Itala, H.T. Aro, Effect of immersion in SBF on porous bioactive bodies made by sintering bioactive glass microspheres, J. Non-Cryst. Solids 275 (2000) 107–115.
[6] L.L. Hench, G.P. LaTorre, The reaction kinetics of bioactive ceramics. Part IV. Effect of glass and solution composition, in: Yamamuro, Kokubo, Nakamura (Eds.), Bioceramics, vol. 5, Kobunshi Kankokai Press, 1993, pp. 67–74.
[7] P. Saravanapavan, J.R. Jones, R.S. Pryce, L.L. Hench, Bioactivity of gel–glass powders in the CaO-SiO_2 system: a comparison with ternary (CaO–P_2O_5–SiO_2) and quaternary glasses (SiO_2–CaO–P_2O_5–Na_2O), J. Biomed. Mater. Res. 66A (2003) 110–119.
[8] A. Oki, B. Parveen, S. Hossain, S. Adeniji, H. Donahue, Preparation and *in vitro* bioactivity of zinc containing sol–gel-derived bioglass materials, J. Biomed. Mater. Res. 69A (2004) 216–221.
[9] R.Z. Domingues, A.E. Clark, A.B. Brennan, A sol–gel derived bioactive fibrous mesh, J. Biomed. Mater. Res. 55 (2001) 468–474.
[10] A. Saboori, M. Rabiee, F. Moztarzadeh, M. Sheikhi, M. Tahriri, M. Karimi, Synthesis, characterization and *in vitro* bioactivity of sol–gel-derived SiO_2–CaO–P_2O_5–MgO bioglass, Mate. Sci. Eng. C 29 (2009) 335–340.
[11] N. Li, Q. Jie, S. Zhu, R. Wang, Preparation and characterization of macroporous sol–gel bioglass, Ceram. Int. 31 (2005) 641–646.
[12] L.L. Hench, et al., Hench, Bioglass and similar materials, Encyclopedia of Materials: Science and Technology, 2001 ISBN: 0-08-0431526, pp. 563–568.
[13] G. Goller, H. Demirkıran, F.N. Oktar, E. Demirkesen, Processing and characterization of bioglass reinforced hydroxyapatite composites, Ceram. Int. 29 (2003) 721–724.

[14] M. Vallet-Regi, J.M. Gonzalez-Calbet, Calcium phosphates as substitution of bone tissues, Prog. Solid State Chem. 32 (2004) 1–31.
[15] X.L. Tang, X.F. Xiao, R.F. Liu, Structural characterization of silicon-substituted hydroxyapatite synthesized by a hydrothermal method, Mater. Lett. 59 (2005) 3841–3846.
[16] I.R. Gibson, S.M. Best, W. Bonfield, Chemical characterization of silicon-substituted hydroxyapatite, J. Biomed. Mater. Res. 44 (1999) 422–428.
[17] K.A. Hing, P.A. Revell, N. Smith, T. Buckland, Effect of silicon level on rate, quality and progression of bone healing within silicate-substituted porous hydroxyapatite scaffolds, Biomaterials 27 (2006) 5014–5026.
[18] T. Gao, H.T. Aro, H. Ylanen, E. Vuorio, Silica-based bioactive glasses modulate expression of bone morphogenetic protein-2 mRNA in Saos-2 osteoblasts in vitro, Biomaterials 22 (12) (2001) 1475–1483.
[19] I.D. Xynos, A.J. Edgar, L.D. Buttery, L.L. Hench, J.M. Polak, Gene expression profiling of human osteoblasts following treatment with the ionic products of Bioglass 45S5 dissolution, J. Biomed. Mater. Res. 55 (2) (2001) 151–157.
[20] J.E. Gough, J.R. Jones, L.L. Hench, Nodule formation and mineralization of human primary osteoblasts cultured on a porous bioactive glass scaffold, Biomaterials 25 (11) (2004) 2039–2046.
[21] F. Balas, J. Perez-Pariente, M. Vallet-Regi, *In vitro* bioactivity of silicon-substituted hydroxyapatites, J. Biomed. Mater. Res. 66A (2003) 364–375.
[22] N. Patel, S.M. Best, W. Bonfield, I.R. Gibson, K.A. Hing, E. Damien, P.A. Revell, A comparative study on the in vivo behaviour of hydroxyapatite and silicon substituted hydroxyapatite granules, J. Mater. Sci. Mater. Med. 13 (2002) 1199–1206.
[23] J.L. Xu, K.A. Khor, Chemical analysis of silica doped hydroxyapatite biomaterials consolidated by a spark plasma sintering method, J. Inorg. Biochem. 101 (2007) 187–195.
[24] A.E. Porter, N. Patel, J.N. Skepper, S.M. Best, W. Bonfield, Comparison of in vivo dissolution processes in hydroxyapatite and silicon-substituted hydroxyapatite bioceramics, Biomaterials 24 (2003) 4609–4620.
[25] E.S. Thian, J. Huang, S.M. Best, Z.H. Barber, W. Bonfield, Magnetron co-sputtered silicon-containing hydroxyapatite thin films—an in vitro study, Biomaterials 26 (2005) 2947–2956.
[26] E.S. Thian, J. Huang, S.M. Best, Z.H. Barber, R.A. Brooks, N. Rushton, W. Bonfield, The response of osteoblasts to nanocrystalline silicon-substituted hydroxyapatite thin films, Biomaterials 27 (2006) 2692–2698.
[27] A.E. Porter, T. Buckland, K. Hing, S.M. Best, W. Bonfield, J. Biomed, The structure of bond between bone and porous silicon-substituted hydroxyapatite bioceramic implants, Mater. Res. A: Appl. Biomater. 78A (2006) 25–33.
[28] A.E. Porter, Nanoscale characterization of the interface between bone and hydroxyapatite implants and the effect of silicon on bone apposition, Micron 37 (2006) 681–688.
[29] M. Palard, E. Champion, S. Foucaud, Synthesis of silicated hydroxyapatite $Ca_{10}(PO_4)_{6-x}(SiO_4)_x(OH)_{2-x}$, J. Solid State Chem. 181 (2008) 1950–1960.
[30] C.M. Botelho, M.A. Lopes, I.R. Gibson, S.M. Best, J.D. Santos, Structural analysis of Si-substituted hydroxyapatite: zeta potential and X-ray photoelectron spectroscopy, J. Mater. Sci. Mater. Med. 13 (2002) 1123–1127.
[31] S.R. Kim, J.H. Lee, Y.T. Kim, D.H. Riu, S.J. Jung, Y.J. Lee, S.C. Chung, Y.H. Kim, Synthesis of Si, Mg substituted hydroxyapatites and their sintering behaviors, Biomaterials 24 (2003) 1389–1398.
[32] S. Hayakawa, K. Tsuru, C. Ohtsuki, A. Osaka, Mechanism of apatite formation on a sodium glass in a simulated body fluid, J. Am. Ceram. Soc. 8 (1999) 2155.
[33] T. Kasuga, Y. Hosoi, M. Nogami, Apatite formation on calcium phosphate invent glasses in simulated body fluid, J. Am. Ceram. Soc. 84 (2001) 450.
[34] T. Kokubo, H. Kushitani, S. Sakka, T. Kitsugi, T. Yamamuro, Solutions able to reproduce *in vivo* surface-structure changes in bioactive glass-ceramic A-W, J. Biomed. Mater. Res. 24 (2004) 721–734.
[35] O. Peitl, E.D. Zanotto, L.L. Hench, Highly bioactive P_2O_5–Na_2O–CaO–SiO_2 glass-ceramics, J. Non-Cryst. Solids 292 (2001) 115–126.
[36] A.J. Salinas, A.I. Martin, M. Vallet-Regi, Bioactivity of three CaO–P_2O_5–SiO_2 sol–gel glasses, J. Biomed. Mater. Res. 61 (2002) 524–532.
[37] P.N. De Aza, J.M. Fernández-Pradas, P. Serra, *In vitro* bioactivity of laser ablation pseudowollastonite coating, Biomaterials 25 (2004) 1983–1990.
[38] C. Sarmento, Z.B. Luklinska, L. Brown, M. Anseau, P.N. De Aza, S. De Aza, F.J. Hughes, I.J. McKay, *In vitro* behavior of osteoblastic cells cultured in the presence of pseudowollastonite ceramic, J. Biomed. Mater. Res. 69A (2004) 351–358.
[39] P.N. De Aza, Z.B. Luklinska, Martinez, M.R. Anseau, F. Guitian, S. De Aza, Morphological and structural study of pseudowollastonite implants in bone, J. Microsc. 197 (2000) 60–67.
[40] P.N. De Aza, Z.B. Luklinska, M.R. Anseau, F. Guitian, S. De Aza, Bioactivity of pseudowollastonite in human saliva, J. Dent. 27 (1999) 107–113.
[41] J.M. Fernández-Pradas, P. Serra, J.L. Morenza, P.N. De Aza, Pulsed laser deposition of pseudowollastonite coatings, Biomaterials 23 (2002) 2057–2061.
[42] H. Yang, C.T. Prewitt, On the crystal structure of pseudowollastonite ($CaSiO_3$), Am. Mineral. 84 (1999) 929–932.
[43] M.A. Lopes, J.D. Santos, F.J. Monteiro, J.C. Knowles, Glass-reinforced hydroxyapatite: a comprehensive study of the effect of glass composition on the crystallography of the composite, J. Biomed. Mater. Res. 39 (1998) 244–251.
[44] F. Moztarzadeh, Electrical conductivity of Y_2O_3 stabilized zirconia, Ceram. Int. 14 (1988) 27–30.